

Bayesian Graphical High-Dimensional Time Series Models for Detecting Structural Changes

Shuvrarghya Ghosh

Department of Statistics, North Carolina State University

Arkaprava Roy

Department of Biostatistics, University of Florida

Anindya Roy

Department of Mathematics and Statistics,

University of Maryland Baltimore County

and

Subhashis Ghosal

Department of Statistics, North Carolina State University

December 5, 2025

Abstract

We study the structural changes in multivariate time-series by estimating and comparing stationary graphs for macroeconomic time series before and after an economic crisis such as the Great Recession. Building on a latent time series framework called Orthogonally-rotated Univariate Time-series (OUT), we propose a shared-parameter framework-the spOUT autoregressive model (spOUTAR)-that jointly models two related multivariate time series and enables coherent Bayesian estimation of their corresponding stationary precision matrices. This framework provides a principled mechanism to detect and quantify which conditional relationships among the variables changed, or formed following the crisis. Specifically, we study the impact of the Great Recession (December 2007–June 2009) that substantially disrupted global and national economies, prompting long-lasting shifts in macroeconomic indicators and their interrelationships. While many studies document its economic consequences, far less is known about how the underlying conditional dependency structure among economic variables changed as economies moved from pre-crisis stability through the shock and back to normalcy. Using the proposed approach to analyze U.S. and OECD macroeconomic data, we demonstrate that spOUTAR effectively captures recession-induced changes in stationary graphical structure, offering a flexible and interpretable tool for studying structural shifts in economic systems.

Keywords: Conditional dependence, Langevin Monte Carlo, Macroeconomic Indicators, Stationary graph

1 Introduction

The Great Recession (December 2007– June 2009) had a profound impact on the global market in several ways. The Great Recession resulted in a prolonged employment slump that persisted long after its official end, as dated by the National Bureau of Economic Research. Unemployment surged, housing prices and stock values collapsed, and over 30 million people lost their jobs, with long-term unemployment doubling its previous record [Song and Von Wachter, 2014]. Household net worth fell significantly [Jacobsen and Mather, 2010]. Consequently, numerous studies examined economic outcomes, such as unemployment’s effects on poverty, inequality, and earnings growth, etc. [Kalleberg and Von Wachter, 2017].

In this paper, we focus on the impact of the Great Recession on the modification and moderation of the relationship between driving economic variables for the US economy [Kalleberg and Von Wachter, 2017] and, more broadly, for the economies of the OECD countries [Ball, 2014]. We investigate changes in the structural associations within the macroeconomic series in the US economy, as well as the cross-country associations in trade, the total economy, and several other key economic indicators.

For stable economies and financial markets, representing implicit associations between variables in multiple economic/financial time series via stationary graphs can be useful and inferentially meaningful Cordini and Sancetta [2024]. However, when potentially systemic shock like the Great Recession happens to economies, the markets and the economic indicators can return to stability with substantial changes to the stationary structure of the series. We study the change in the stationary graph among the associated variables before and after the Great Recession via estimation of stationary precision matrices and comparison of the forms. For our investigation, the economies are assumed to be stable before the recession and also in the period following the event when

sufficient time has passed for economies to return to normalcy.

We adopt the multivariate time series framework, the Orthogonally-rotated Univariate Time-series (OUT) model [Roy et al., 2024], which facilitates the estimation of stationary graphs for multivariate time series. However, we look for the expected change in the stationary graph due to the economic shock. Thus, we are dealing with two potentially related multivariate time series and want to compare the stationary graphs associated with the two series; we propose a shared-parameter-OUT (spOUT) model. The univariate time series are modeled as autoregressive processes, and thus we call our final model spOUTAR. We apply this framework to estimate the stationary graphs before and after the crisis. Consequently, our interest lies in learning the changes in the underlying stationary graphs. In this context, the variables denote vertices of an undirected graph, and an edge between two vertices denotes their conditional dependency on each other when controlling for the other variables. Finally, the scientific goal is also to identify which conditional relationships have strengthened or weakened after the Great Recession. We define these quantities within our Bayesian framework.

The remainder of the article is organized as follows. In Section 3, we describe the spOUTAR model, which covers our choice of prior distributions and the specification of the posterior sampling strategy. Then, in Section 4, we discuss the numerical results obtained through simulation studies and real data analyses. Finally, we conclude the paper in Section 5.

2 Data and Exploratory analysis

In this article, we analyze two macroeconomic datasets. A brief description of each, along with some preliminary exploratory data analysis, is provided below.

1. *OECD nations GDP dataset*: The Organization for Economic Co-operation and Development

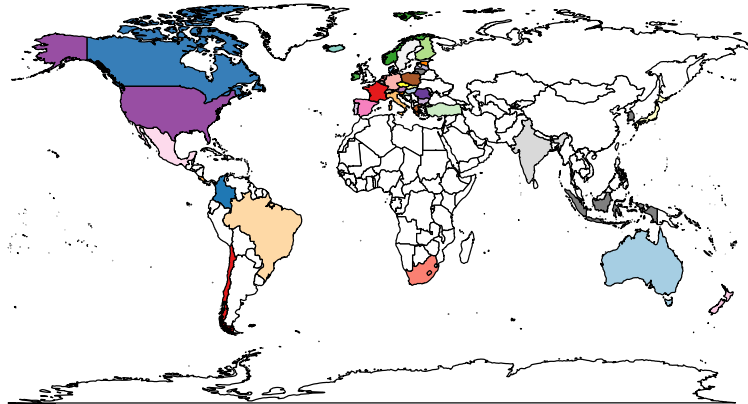
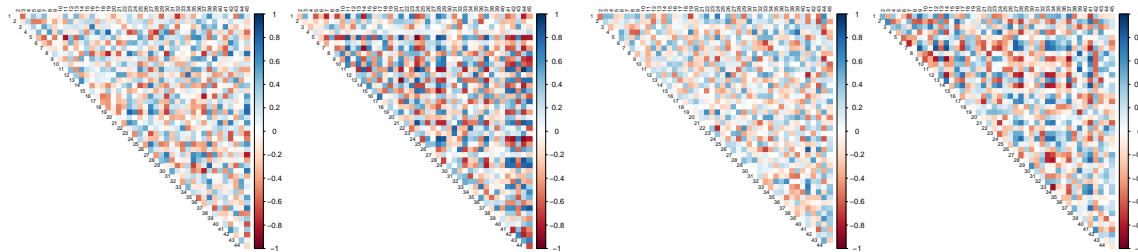


Figure 1: OECD countries. The GDP and its components are studied for all the countries that are highlighted in the map.

(OECD) has 38 member countries, primarily consisting of developed nations with market-based economies. In this analysis, we use quarterly Gross Domestic Product (GDP) data from the OECD member countries along with a few additional nations, totaling 45 in all. The data, expressed in US dollars, is based on the expenditure approach, which computes GDP as the sum of the following components: final consumption expenditure of households and nonprofit institutions serving households (NPISH), final consumption expenditure of general government, gross fixed capital formation (i.e., investment), and net exports (exports minus imports). In addition to analyzing GDP, we also examine each of these components individually. To develop an elementary understanding of pairwise dependencies among variables, while controlling for the effects of other variables and ignoring temporal dependence in each variable, we compute the partial correlation coefficients for every pair of variables in each data component. Two heatmaps illustrating the partial correlations among import trade variables and export trade variables are presented in Figure 2a and Figure 2b respectively. The remaining

plots are displayed in Appendix.

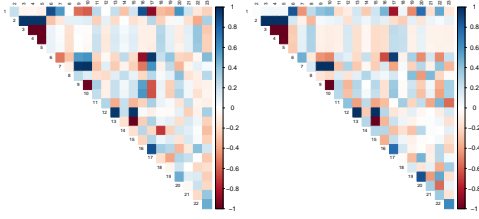


(a) Partial correlations among import trade features: before (left) vs. after (right) the recession. (b) Partial correlations among export trade features: before (left) vs. after (right) the recession.

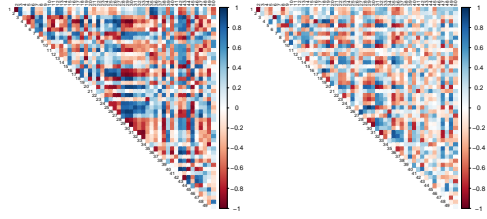
Figure 2: Changes in the partial correlations of (a) import trade features and (b) export trade features, following the Great Recession.

2. *FRED-QD macroeconomic dataset*: This quarterly macroeconomic data from the Federal Bank of St. Louis, comprising 248 quarterly time series, closely resembles the Stock-Watson datasets (see [Stock and Watson \[2006, 2012\]](#)), and is classified into 14 groups. We consider 5 groups for our analysis: National Income and Product Accounts (NIPA, 23 variables); Industrial production (16 variables); Employment and unemployment (50 variables); Housing (13 variables); and Prices (48 variables). We pre-process the data as instructed in [McCracken and Ng \[2020\]](#) and carry out the analysis in a similar way as outlined in Section 4.1.1. Similar to the OECD data, we examine the partial correlations for each component of this dataset. Heatmaps for the NIPA and Employment and Unemployment components are displayed in Figure 3a and Figure 3b, respectively.

The exploratory data analyses show appreciable changes in the partial correlation structure



(a) Partial correlations among NIPA variables: before (left) vs. after (right) the recession.



(b) Partial correlations among employment and unemployment attributes: before (left) vs. after (right) the recession.

Figure 3: Changes in partial correlations between key macroeconomic indicators: (a) NIPA variables, and (b) employment/unemployment attributes, following the Great Recession.

among our macroeconomic variables of interest, albeit ignoring the time series nature of the data. Since the two periods involve the same set of macroeconomic variables, we propose a shared-parameter model tailored for studying structural changes in paired multivariate time series data.

3 Method

We write $[n]$ to denote the set $\{1, 2, \dots, n\}$, for any $n \in \mathbb{N}$, the set of natural numbers. The notation $\text{vec} : \mathbb{R}^{r \times s} \rightarrow \mathbb{R}^{rs}$ denotes the vectorization operator, a linear map that transforms a matrix $\mathbf{X} \in \mathbb{R}^{r \times s}$ to a $rs \times 1$ -dimensional vector by stacking the columns of \mathbf{X} on top of one another. Let $\|\mathbf{X}\|_F$ denote the Frobenius norm of matrix \mathbf{X} given by the relation $\|\mathbf{X}\|_F = \sqrt{\sum_{i,j} X_{ij}^2}$. Let $\text{diag}(x_1, \dots, x_d)$ be a d -dimensional diagonal matrix with diagonal entries $\{x_1, \dots, x_d\}$, and let $\boldsymbol{\sigma} = (\sigma_1, \dots, \sigma_p)$ be the vector of innovation variances for the AR processes. Finally, we write

$N(\mu, \sigma^2)$ to denote a univariate normal distribution with mean $\mu \in \mathbb{R}$ and variance σ^2 , $\sigma > 0$; $\text{Unif}(a, b)$ to denote a uniform distribution with finite support $(a, b) \subset \mathbb{R}$; $\text{Logistic}(\mu, \sigma)$ to denote a logistic distribution with location $\mu \in \mathbb{R}$ and scale $\sigma > 0$; $\text{InvGamma}(\alpha, \beta)$ to denote an inverse gamma distribution with shape $\alpha > 0$ and scale $\beta > 0$; and $\text{InvGauss}(\mu, \tau)$ to denote an inverse Gaussian distribution with mean $\mu > 0$ and shape $\tau > 0$.

Consider a multivariate time series $\mathbf{Y} \in \mathbb{R}^{p \times (n_1 + n_2)}$ with p variables, each having n_0 observations, where it contains a period of disruption, such as the Great Depression and there are n_1 time points in period 1 (before the crisis) and n_2 time points in period 2 (after the crisis). Consequently, we form two data matrices $\mathbf{Y}_1 \in \mathbb{R}^{p \times n_1}$, and $\mathbf{Y}_2 \in \mathbb{R}^{p \times n_2}$. Let $\mathbf{\Sigma}_1$ and $\mathbf{\Sigma}_2$ denote the $p \times p$ dispersion matrices of \mathbf{Y}_1 and \mathbf{Y}_2 respectively. Then, using the framework in Roy et al. [2024], \mathbf{Y}_1 and \mathbf{Y}_2 can be expressed as

$$\mathbf{Y}_1 = \mathbf{\Sigma}_1^{1/2} \mathbf{U} \mathbf{Z}_1 \text{ and } \mathbf{Y}_2 = \mathbf{\Sigma}_2^{1/2} \mathbf{U} \mathbf{Z}_2$$

respectively. Since $\mathbf{\Sigma}_1$ and $\mathbf{\Sigma}_2$ are positive definite matrices, we write $\mathbf{\Sigma}_1^{1/2}$ and $\mathbf{\Sigma}_2^{1/2}$ to denote their respective Cholesky square roots. Let $\mathbf{Z}_1 \in \mathbb{R}^{p \times n_1}$ and $\mathbf{Z}_2 \in \mathbb{R}^{p \times n_2}$ be two matrices with p independent latent variables, each representing a univariate time series with unit marginal variance. The variable \mathbf{U} is a $p \times p$ orthogonal matrix that ensures order independence as we are using the Cholesky decomposition of the dispersion matrices to define the square root.

We assume that the observations of the i th row of \mathbf{Z}_1 and \mathbf{Z}_2 are assumed to be part of the same univariate time series for all $i = [p]$. However, due to the substantial gap between the two periods, they become independent but with the same underlying time series characterization parameters. We assume that each univariate time series follows an autoregressive (AR) process for all $i = [p]$. The orders of the AR processes may be different for different univariate processes. For simplicity, unless otherwise stated, we assume a uniform order q for all throughout this article.

Let the t_1 th time point of \mathbf{Y}_1 be expressed as $\mathbf{Y}_{1,t_1} = \boldsymbol{\Sigma}_1^{1/2} \mathbf{U} \mathbf{Z}_{1,t_1}$, for any $t_1 \in [n_1]$. Based on the relationship between \mathbf{Y}_1 and \mathbf{Z}_1 , it is immediate that $\mathbf{Z}_{1,t_1} = \mathbf{U}^T \boldsymbol{\Omega}_1^{1/2} \mathbf{Y}_{1,t_1}$, where $\boldsymbol{\Omega}_1 = \boldsymbol{\Sigma}_1^{-1}$. Since $\boldsymbol{\Omega}_1$ is a symmetric positive definite matrix, we can write $\boldsymbol{\Omega}_1 = (\mathbf{I} - \mathbf{L}_1) \mathbf{D}_1^2 (\mathbf{I} - \mathbf{L}_1)^T$, where \mathbf{D}_1 is a diagonal matrix and \mathbf{L}_1 is a strictly lower-triangular matrix. Consequently, its Cholesky square root is $\boldsymbol{\Omega}_1^{1/2} = (\mathbf{I} - \mathbf{L}_1) \mathbf{D}_1$. Similarly, for the t_2 th time point of \mathbf{Y}_2 , $\mathbf{Z}_{2,t_2} = \mathbf{U}^T \boldsymbol{\Omega}_2^{1/2} \mathbf{Y}_{2,t_2}$, for any $t_2 \in [n_2]$, $\boldsymbol{\Omega}_2 = \boldsymbol{\Sigma}_2^{-1}$, and $\boldsymbol{\Omega}_2^{1/2} = (\mathbf{I} - \mathbf{L}_2) \mathbf{D}_2$. In our proposed method, we assume $\boldsymbol{\Omega}_1$ and $\boldsymbol{\Omega}_2$ share a common diagonal matrix such that $\mathbf{D}_1 = \mathbf{D}_2 = \mathbf{D}$, and differ only in \mathbf{L}_1 and \mathbf{L}_2 that control the underlying connectivity patterns. Since $\boldsymbol{\Omega}_1$ gives the conditional dependency structure before the crisis, and $\boldsymbol{\Omega}_2$ gives the structure post-crisis, their difference, $\boldsymbol{\Omega}_2 - \boldsymbol{\Omega}_1$, reveals changes in the dependency structure following the crisis.

Let the coefficient vector of the i -th AR process be $\boldsymbol{\varphi}_i = (\varphi_{i,1}, \dots, \varphi_{i,q})^T$, $i = [p]$. Then, the coefficient matrix for all the AR processes combined is denoted by $\boldsymbol{\Psi} = (\boldsymbol{\varphi}_1, \dots, \boldsymbol{\varphi}_p)^T$. Similarly, let the autocorrelation functions (acf) and partial autocorrelation functions (pacf) of the i -th time series be respectively defined by $\boldsymbol{\gamma}_i = (\gamma_{i,1}, \dots, \gamma_{i,q})^T$ and $\boldsymbol{\rho}_i = (\rho_{i,1}, \dots, \rho_{i,q})^T$ where $i = [p]$.

We assume that the individual processes are subject to stationarity and causality constraints. In other words, we parameterize the AR process in terms of its pacf parameters $\boldsymbol{\rho}_i = \{\rho_{i,k}\}_{k=1}^q$, with $\rho_{i,k} \in [-1, 1]$, for any $i \in [p]$ and all $k = [q]$. Subsequently, we obtain the AR process parameters, including the innovation variances, by applying the Durbin-Levinson recursion algorithm and the Yule-Walker equations as follows. To get the AR coefficients $\boldsymbol{\varphi}_i = (\varphi_{i,1}, \dots, \varphi_{i,q})$ from $\boldsymbol{\rho}_i$, we apply the the Durbin-Levinson algorithm. Then the implied $\boldsymbol{\gamma}_i$ is obtained from $\boldsymbol{\varphi}_i$ using the Yule-Walker equations. Finally, the innovation variance is obtained by the relation $\sigma_i^2 = 1 - \sum_{k=1}^q \gamma_{i,k} \varphi_{i,k}$, ensuring that the marginal variances are 1. We denote the vector of p innovation variances by $\boldsymbol{\sigma} = (\sigma_1, \dots, \sigma_p)$.

Furthermore, we assume that the white noise in each AR process follows a normal distribution.

Then, the t -th observation of the i -th component of \mathbf{Z}_1 is modeled as

$$Z_{1,i,t} = \sum_{k=1}^q \varphi_{i,k} Z_{1,i,t-k} + \varepsilon_i, \quad \text{for all } i \in [p]; t \in \{q+1, \dots, s\},$$

where $\varepsilon_i \sim \mathcal{N}(0, \sigma_i^2)$ i.i.d. and the model above can be viewed as a linear regression model. We ignore the first q observations in each time series. The corresponding log-likelihood for the time-series $Z_{1,i}$ is

$$\log \pi(\varphi_i, \sigma_i | Z_{1,i}) \propto -\frac{1}{2\sigma_i^2} \sum_{t=q+1}^s (Z_{1,i,t} - \sum_{k=1}^q \varphi_{i,k} Z_{1,i,t-k})^2, \quad i = [p].$$

Consequently, the joint log-likelihood of all p AR processes in \mathbf{Z}_1 is

$$\log \pi(\Psi, \sigma | \mathbf{Z}_1) \propto -\sum_{i=1}^p \frac{1}{2\sigma_i^2} \sum_{t=q+1}^{n_1} (Z_{1,i,t} - \sum_{k=1}^q \varphi_{i,k} Z_{1,i,t-k})^2. \quad (1)$$

Similarly, for \mathbf{Z}_2 ,

$$\log \pi(\Psi, \sigma | \mathbf{Z}_2) \propto -\sum_{i=1}^p \frac{1}{2\sigma_i^2} \sum_{t=q+1}^{n_2} (Z_{2,i,t} - \sum_{k=1}^q \varphi_{i,k} Z_{2,i,t-k})^2. \quad (2)$$

To draw posterior samples of \mathbf{L}_1 , we use the expression in (1), thus using the data from the pre-crisis period only. Similarly, for \mathbf{L}_2 , we use the expression in (2), involving the data from the post-crisis period. For all other parameters, we use the combined log-likelihood obtained by adding the expressions in the preceding two displays. Further computational details are described in the following subsections.

Since $\mathbf{\Omega}_1 = (\mathbf{I} - \mathbf{L}_1)\mathbf{D}^2(\mathbf{I} - \mathbf{L}_1)^T$ and $\mathbf{\Omega}_2 = (\mathbf{I} - \mathbf{L}_2)\mathbf{D}^2(\mathbf{I} - \mathbf{L}_2)^T$, we induce priors on $\mathbf{\Omega}_1$ and $\mathbf{\Omega}_2$ by placing independent priors on \mathbf{D} , \mathbf{L}_1 , and \mathbf{L}_2 . We restrict \mathbf{D} to have positive diagonal entries only, and \mathbf{L}_1 and \mathbf{L}_2 are strictly lower-triangular by definition. We assume $\mathbf{\Omega}_1$ and $\mathbf{\Omega}_2$ to be sparse matrices and induce it by making \mathbf{L}_1 and \mathbf{L}_2 sparse. Our complete set of parameters is $\{\mathbf{D}, \mathbf{L}_1, \mathbf{L}_2, \mathbf{U}, \Psi\}$.

We take a Bayesian route by assigning priors to all the model parameters, as discussed in the next subsection. The posterior distribution is then approximated using a Markov chain Monte Carlo (MCMC) algorithm. Finally, we use the MCMC samples to characterize both the magnitude and direction of changes in connectivity.

3.1 Prior specification

The prior specifications for the Cholesky parameters and the orthogonal matrix in this article are similar to those used in Roy et al. [2024]. However, we include the complete prior specification in this paper for the sake of completeness.

- *Prior for \mathbf{D}* : Define $\mathbf{D} = \text{diag}(d_1, \dots, d_p)$ where each diagonal element is independently distributed as $\text{InvGauss}(\xi, 1)$. This prior has an exponential-like tail near both zero and infinity. Lastly, we put a prior distribution $N(0, \sigma_d^2)$ on ξ and set σ_d to some large constant to make the prior weakly-informative.
- *Prior for \mathbf{L}_1 and \mathbf{L}_2* : Each sub-diagonal component of \mathbf{L}_1 is independently distributed as $H_{\lambda_{\mathbf{L}_1}}(X)$ given $\lambda_{\mathbf{L}_1}$, where $X \sim N(0, \sigma_{\mathbf{L}_1}^2)$, $H_{\lambda_{\mathbf{L}_1}}(x) = x \mathbb{1}\{|x| > \lambda_{\mathbf{L}_1}\}$ is the hard-thresholding operator at level $\lambda_{\mathbf{L}_1}$ and $\lambda_{\mathbf{L}_1} \sim \text{Unif}(0, 100)$. Further, we put an $\text{InvGamma}(0.01, 0.01)$ prior on $\sigma_{\mathbf{L}_1}^2$. Similarly, we put priors on \mathbf{L}_2 , $\lambda_{\mathbf{L}_2}$, and $\sigma_{\mathbf{L}_2}^2$.
- *Prior for \mathbf{U}* : Using the Cayley representation for the special orthogonal matrices, we can reparametrize $\mathbf{U} = (\mathbf{I} - \mathbf{A})(\mathbf{I} + \mathbf{A})^{-1}$ where \mathbf{A} is a skew-symmetric matrix. A skew-symmetric matrix \mathbf{A} has all diagonal entries zero, and sub-diagonal entries are unrestricted. We assume \mathbf{A} to be sparse and the sparsity of \mathbf{A} is achieved by specifying a thresholding-based prior for the sub-diagonal entries similar to that used for \mathbf{L}_1 and \mathbf{L}_2 . The sub-diagonal entries of \mathbf{A} are independently distributed as $H_{\lambda_{\mathbf{A}}}(X)$ given $\lambda_{\mathbf{A}}$, where $X \sim N(0, \sigma_{\mathbf{A}}^2)$, $H_{\lambda_{\mathbf{A}}}(x) =$

$x\mathbb{1}\{|x| > \lambda_{\mathbf{A}}\}$ is the hard-thresholding operator at level $\lambda_{\mathbf{A}}$ and $\lambda_{\mathbf{A}} \sim \text{Unif}(0, 100)$. We put an $\text{InvGamma}(0.1, 0.1)$ prior on $\sigma_{\mathbf{A}}^2$.

- *Prior for Ψ* : To maintain stationarity and causality constraints on the AR parameters, we put $\text{Unif}(-1, 1)$ priors on the corresponding pacfs $\rho_{i,1}, \dots, \rho_{i,K}$ for $i = 1, 2, \dots, p$ and apply the Durbin-Levinson algorithm to map them back to the AR parameters and innovation variance assuming unit marginal variance.

3.2 Sampling from the posterior

Model initialization: To start the MCMC chain from a reasonable starting value, we use a hot start in the following manner.

1. To initialize $\mathbf{\Omega}_1$ and $\mathbf{\Omega}_2$, we use the precision matrix estimates $\hat{\mathbf{\Omega}}_1$ and $\hat{\mathbf{\Omega}}_2$ (say) obtained from the output of the Gaussian graphical model (GGM; see [Mohammadi and Wit \[2015\]](#)) fit to the pre-crisis data and post-crisis data respectively. The GGM model is implemented using the `bdgraph` package in R [[Mohammadi and Wit, 2019](#)]. This step ignores the across-time dependence. Subsequently, we compute the modified Cholesky factorization of $\hat{\mathbf{\Omega}}_1$ to get $\hat{\mathbf{L}}_1$ and $\hat{\mathbf{D}}_1$, and of $\hat{\mathbf{\Omega}}_2$ to get $\hat{\mathbf{L}}_2$ and $\hat{\mathbf{D}}_2$.
2. Initialize $\mathbf{L}_1 = \hat{\mathbf{L}}_1$, $\mathbf{L}_2 = \hat{\mathbf{L}}_2$, and $\mathbf{D} = (\hat{\mathbf{D}}_1 + \hat{\mathbf{D}}_2)/2$. Set $\mathbf{A} = \mathbf{0}$ so that $\mathbf{U} = \mathbf{I}$. Obtain \mathbf{Z}_1 using the relation $\mathbf{Z}_1 = \mathbf{U}^T \mathbf{D} (\mathbf{I} - \mathbf{L}_1) \mathbf{Y}_1$, and \mathbf{Z}_2 from the relation $\mathbf{Z}_2 = \mathbf{U}^T \mathbf{D} (\mathbf{I} - \mathbf{L}_2) \mathbf{Y}_2$.
3. Initialize the AR coefficients of all the p AR processes using the `ar()` function in R. Compute the acf and pacfs of the corresponding coefficients using `inla.ar.phi2acf()` and `inla.ar.phi2pacf()` functions from the R package INLA by [Gómez-Rubio \[2020\]](#).
4. Set $\lambda_{\mathbf{A}} = \lambda_{\mathbf{L}_1} = \lambda_{\mathbf{L}_2} = 0$. Initialize $\sigma_{\mathbf{A}}^2$, $\sigma_{\mathbf{L}_1}^2$ and $\sigma_{\mathbf{L}_2}^2$ using draws from the inverse gamma

posterior based on initial values of $\text{vec}(\mathbf{A})$, $\text{vec}(\mathbf{L}_1)$ and $\text{vec}(\mathbf{L}_2)$

MCMC sampling: Considering the structure of the model and the prior specification, the posterior is not completely analytically tractable. Hence, we use Metropolis-Hastings (M-H) and Metropolis-adjusted Langevin Monte Carlo (MALA) algorithms to sample from the posterior. The AR coefficients have causality and stationarity constraints on them and hence we sample only the AR parameters for the first 1500 iterations keeping \mathbf{L}_1 , \mathbf{L}_2 , \mathbf{D} and \mathbf{A} fixed to their initial values. After the AR parameters have stabilized, we start sampling the the values of \mathbf{L}_1 , \mathbf{L}_2 , \mathbf{D} and \mathbf{A} with $\lambda_{\mathbf{A}}$ and $\lambda_{\mathbf{L}_1}, \lambda_{\mathbf{L}_2}$ fixed to zero until another 1000 iterations. Further, it is important to note that hard spike-and-slab priors on the entries of \mathbf{L}_1 , \mathbf{L}_2 and \mathbf{A} are computationally expensive. Therefore while sampling, we use a computationally convenient modification of the prior through hard or soft-thresholding as described below.

For the matrix \mathbf{A} , we let a sub-diagonal entry $a_{ij}, i > j$, be distributed as $S_{\lambda'}(X) := X(1 - \lambda'/|X|)_+$, where $X \sim \mathcal{N}(0, \sigma_T^2)$ and λ' is a hyperparameter, independently of other sub-diagonal entries. Then it follows that for all $i > j$,

$$a_{ij} | \lambda' \sim \begin{cases} \delta_0, & \text{with probability } \Phi\left(\frac{\lambda'}{\sigma_T}\right) - \Phi\left(-\frac{\lambda'}{\sigma_T}\right); \\ \phi\left(\frac{|a_{ij}| + \lambda'}{\sigma_T} \text{sign}(a_{ij})\right), & \text{otherwise.} \end{cases}$$

Finally, we put a prior $\lambda' \sim \text{Unif}(\lambda_l, \lambda_u)$. We set $\lambda_l = 0$ and λ_u to some large constant.

We use Gibbs sampling to sample $\mathbf{D}, \mathbf{L}_1, \mathbf{L}_2, \mathbf{A}$ and Ψ . To initialize the chain, we use a hot starting point based on the estimated values of the parameters.

- *Sampling the matrix \mathbf{A} :* We consider Metropolis-Hastings (M-H) moves for the lower-triangular entries \mathbf{A} . Specifically, we propose a small additive movement in \mathbf{A} from its initial position using realizations from a multivariate normal distribution whose mean is the previous accepted

value and covariance matrix is some scalar multiple of identity.

- *Sampling the matrices \mathbf{L}_1 and \mathbf{L}_2 :* We use Metropolis-adjusted Langevin algorithm (MALA) to update \mathbf{L}_1 and \mathbf{L}_2 . MALA combines aspects of the M-H algorithm with Langevin dynamics, enhancing efficiency by leveraging gradient information of the target distribution. The algorithm updates sample positions by adding a drift term, based on the gradient of the logarithm of the target density, to a random Gaussian noise term. This gradient-guided proposal step encourages movement toward regions of higher probability, thus reducing random walk behavior common in other MCMC methods. Each proposed sample is accepted or rejected based on the M-H criterion [Roberts and Stramer, 2002].

Computing the gradient of the hard-thresholding operator is difficult due to its discontinuity. Thus, we approximate the thresholding operator by $\mathbb{1}\{|x| > \lambda\} \approx \{1 + 2\pi^{-1} \tan^{-1}((x^2 - \lambda^2)/h_0)\} / 2$ [Cai et al., 2020], with h_0 chosen as a small number such as 10^{-8} . This helps in a gradient-based updating of \mathbf{L}_1 and \mathbf{L}_2 . The gradient of the likelihood with respect to \mathbf{L}_1 and \mathbf{L}_2 can be found in Appendix A.1.2.

- *Sampling the matrix \mathbf{D} :* Likewise, as in the last step, we use a MALA routine to sample elements of \mathbf{D} . Due to the positivity constraint on diagonal elements of \mathbf{D} , we update this parameter in the log scale with the necessary Jacobian adjustment. The gradient of the likelihood with respect to \mathbf{D} used to compute the Langevin diffusion is given in Appendix A.1.3.
- *Sampling the AR parameters:* Note that the AR processes are independent and are parametrized in terms of pacfs, which are bounded in $(-1, 1)$.

We update these parameters using the M-H algorithm. Here, we again reparameterize the pacf parameters for i -th AR process, ρ_i , as $\log((\rho_i + 1)/2) = \mathbf{V}_i$ (say). Then, the uniform

prior on the components of φ_i induces Logistic(0,1) prior on the components of \mathbf{V}_i with unrestricted support. This allows implementing the adaptive M-H algorithm to update the \mathbf{V}_i 's following Haario et al. [2001]. To map the pacf parameter back to the AR parameters, the R function `inla.ar.pacf2phi()` from INLA package will be used.

- *Sampling the thresholding parameters* : We update $\lambda_{\mathbf{L}_1}$ and $\lambda_{\mathbf{L}_2}$ using a random walk M-H step in the log scale with a Jacobian adjustment every 20th iteration. $\lambda_{\mathbf{A}}$ is also updated similarly for every 30th iteration. Update $\sigma_{\mathbf{L}_1}^2$, $\sigma_{\mathbf{L}_2}^2$ and $\sigma_{\mathbf{A}}^2$ accordingly using updated values of $\text{vec}(\mathbf{L}_1)$, $\text{vec}(\mathbf{L}_2)$ and $\text{vec}(\mathbf{A})$ using draws from the inverse gamma posterior distribution.

We draw a total of 10000 samples and discard the first 5000 as burn-in. In the first 1500 iterations, we only update the AR process parameters, keeping all the other ones fixed to their initializations. Subsequently, we start updating \mathbf{L}_1 , \mathbf{L}_2 , \mathbf{D} , and \mathbf{A} , keeping the values of the thresholding parameters set to zero for the next 1000 iterations. Then, from the 2500-*th* iteration onwards, we start updating all the parameters. Note that these adjustments are done during the burn-in phase of the MCMC. The above-mentioned iteration numbers are carefully selected through our extensive numerical experiments. For the M-H algorithm, the acceptance rate is maintained between 15–40% by rescaling the magnitude of the variances of the proposals accordingly for every 100-*th* iteration to ensure adequate mixing. Similarly, for MALA, it is kept between 45–70% by adjusting the step size parameter at every 100-*th* iteration.

Prediction: Suppose that we want to predict the value of \mathbf{Y}_T , for some $T > n$. Following the burn-in period of the sampler, in the i th MCMC iteration and for AR order q , we sequentially compute

$$\mathbf{Y}_{t,i}^* = \boldsymbol{\Sigma}_i^{1/2} \mathbf{U}_i \mathbf{Z}_{t,i}, \text{ where } \mathbf{Z}_{t,i} = \mathbf{Z}_{t:t-q} \boldsymbol{\Psi} + \boldsymbol{\sigma}; \text{ for all } t \in \{n+1, \dots, T\}.$$

Consequently, the posterior mean estimate of \mathbf{Y}_T is given by $\hat{\mathbf{Y}}_T = \sum_i \mathbf{Y}_{T,i}^*/N$, where N is the

number of iterations of MCMC excluding the burn-in period. Clearly, for one-step-ahead predictions, we take $T = n + 1$.

Posterior inference on connectivity changes: We first calculate the posterior samples of the differences in the precision matrices $\mathbf{\Omega}_{21} = \mathbf{\Omega}_2 - \mathbf{\Omega}_1$ (say) by computing this difference for each posterior sample and then determine the 95% credible interval for each entry. An edge is classified as having a positive (negative) shift if the two nodes it connects share a stronger (weaker) relationship following the period of crisis. In practice, we identify an edge to have a positive (negative) shift if its credible interval lies entirely in the positive (negative) region of the real line. We will use blue lines to indicate positive shifts and red lines to indicate negative shifts in the graphs displayed in this section, the next section, and in the appendix. The adjacency matrix is then constructed by assigning edges to those node pairs for which the credible interval of the corresponding entry of $\mathbf{\Omega}_{21}$ excludes zero.

4 Numerical studies

In this section, we present the results of the real data analyses, and evaluate the predictive performance of the model besides assessing the underlying graphical structure in the data via various simulation settings.

4.1 Real data analysis

We analyze the dynamic characteristics of the macroeconomic components of the Gross Domestic Product (GDP) series before and after the Great Recession. The great recession began in December 2007 and lasted until June 2009. To compare the behavior of the series before and after the great recession we split each series into two parts, one before December 2007 and the other after July

2009. We use two real datasets that are updated in real time. In both cases, we also compare the one-step ahead predictive performance of our method with that of the sparse vector autoregressive model (VAR) (see Lütkepohl [2013], Basu and Michailidis [2015]) where the sparse VAR forecasts are obtained using the `sparsevar` R package. In addition, we illustrate the underlying graphical structure using the estimated precision matrices and discuss the resilience of the connections between different economic factors based on the differences in the estimated marginal precisions from before and after recession periods. Throughout the following sections, the sparse VAR model will be called “Sparse-VAR”.

4.1.1 Quarterly GDP data of OECD nations

We consider data from the quarter 1 (Q1) of 1998 to Q4 of 2019, excluding data from the recession period 2007 Q4 to 2009 Q3. In each case, we model the first difference of the natural logarithm of the series to remove any longtrend. Small scaling adjustments have been made to avoid numerical instabilities. Subsequently, we fit Sparse-VAR and spOUTAR models of orders 2 through 8, and present the root mean squared errors in Table 1.

The prediction error for the 2019 Q4 time point is computed using only Ω_2 . The spOUTAR model outperforms the Sparse-VAR model in all cases, indicating superior predictive performance. To construct the graph adjacency matrix for each case, we follow the approach discussed at the end of the previous subsection based on the posterior samples of $\Omega_{21} = \Omega_2 - \Omega_1$. Next, we compute the posterior mean of the difference, $\bar{\Omega}_{21}$; extract the values corresponding to the edges in the adjacency matrix; sort these values in descending order; and report the top 10 edges in Table 2.

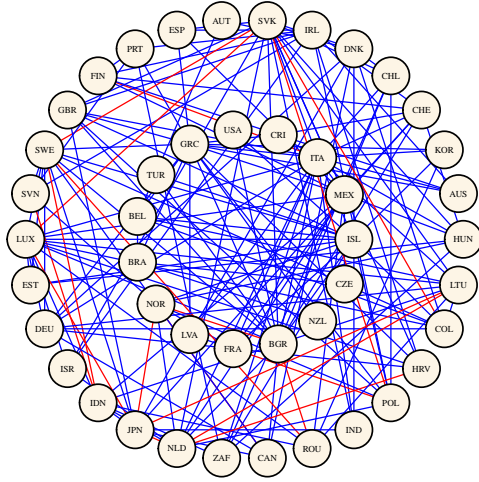
The total GDP and its components exhibit a rich graphical dependency structure. We analyze the graphical patterns in the import and export trade data, as shown in Figure 4a and Figure 4b respectively. Additional graphs and the names of the OECD countries corresponding to the numeric

Table 1: One-step prediction errors of Sparse-VAR and spOUTAR models for different orders of autoregressive processes for OECD-QD data.

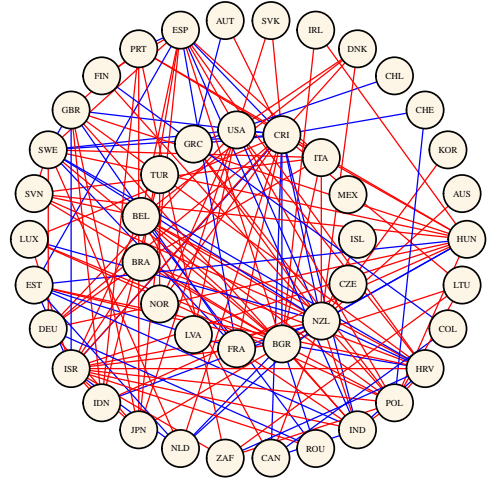
GDP Component (USD)	Model	q						
		2	3	4	5	6	7	8
Total Economy	Sparse-VAR	0.1210	0.1154	0.1233	0.1219	0.1275	0.1275	0.1275
	spOUTAR	0.0092	0.0105	0.0098	0.0096	0.0096	0.0102	0.0099
Import expenditure	Sparse-VAR	1.5221	1.5372	1.5632	1.5656	1.4395	1.3874	1.0003
	spOUTAR	0.0738	0.0729	0.0714	0.0757	0.0696	0.0692	0.0742
Export expenditure	Sparse-VAR	1.3968	1.3968	1.0550	1.3946	1.3968	1.3968	1.3968
	spOUTAR	0.0277	0.0262	0.0272	0.0275	0.0271	0.0289	0.0269
Total capital expenditure	Sparse-VAR	3.5345	3.5695	4.3061	2.8892	3.6046	2.8249	2.1092
	spOUTAR	0.1477	0.1467	0.1544	0.1633	0.1576	0.1653	0.1751
General government expenditure	Sparse-VAR	1.0361	0.6447	0.6457	0.6504	0.5276	0.4800	0.3851
	spOUTAR	0.0255	0.0222	0.0194	0.0229	0.0231	0.0211	0.0176
Household expenditure	Sparse-VAR	0.1628	0.1599	0.1628	0.1628	0.1628	0.1521	0.1500
	spOUTAR	0.0160	0.0151	0.0158	0.0158	0.0157	0.0155	0.0208

Table 2: Edges that exhibit top 10 conditional dependencies in OECD-QD data groups based on the sorted absolute differences in the posterior mean of Ω_{21} .

Group	Dependencies (edges)
Total economy	(IDN, JPN), (SWE, JPN), (LVA, JPN), (LUX, IND), (AUS, GBR), (AUS, CHE), (CAN, LTU), (ISR, JPN), (AUS, JPN), (AUS, CHL)
Import expenditure	(COL, LTU), (SVK, NLD), (MEX, ITA), (BGR, NLD), (ITA, LVA), (MEX, HUN), (BGR, IDN), (BGR, GBR), (LUX, LTU), (MEX, SVK)
Export expenditure	(CRI, AUT), (CRI, HUN), (BGR, LUX), (ESP, HRV), (NZL, FIN), (ESP, SWE), (FIN, COL), (IND, HRV), (BEL, ISR), (ESP, POL)
Total capital expenditure	(ITA, COL), (GRC, FIN), (FIN, IND), (NOR, PRT), (LVA, DEU), (ISL, ESP), (IND, POL), (ESP, FIN), (LVA, CHE), (ITA, IND)
General government expenditure	(BGR, CHE), (CHE, SVK), (SVK, HRV), (NZL, HRV), (NOR, IND), (BEL, IND), (IND, HRV), (USA, BEL), (HRV, LTU), (BGR, KOR)
Household expenditure	(AUS, KOR), (USA, GBR), (GBR, SWE), (USA, AUS), (SWE, NLD), (PRT, JPN), (BEL, SWE), (CZE, KOR), (IDN, JPN), (BGR, KOR)



(a) Overall *positive shifts* in import trade relations, highlighting stronger correlations among the trading partners; using spOUTAR with order 7.



(b) Overall *negative shifts* in export trade relations, highlighting weaker correlations among the trading partners; using spOUTAR with order 3.

Figure 4: Shifts in trade dynamics among the OECD nations following the Great Recession [Dec 2007 - Jun 2009]: (a) import trade volumes and (b) export trade volumes.

labels in the nodes of each graph are displayed in Appendix A.3. Both import and export trade graphs reveal significant cross-country dependence. According to the World Trade Organization (WTO), global trade volumes declined by approximately 12% during the recession. Following the crisis, global trade experienced a strong rebound, though it did not surpass pre-crisis levels until 2012, after which the economies grew more slowly compared to pre-recession trends. Our analysis indicates that the import trade graph displays an overall positive shift, whereas the export trade graph shows a predominantly negative shift. The contrasting pattern in both graphs suggests significant changes in trade relationships and policies among the 45 countries following the crisis. Another possible reason can be the uneven recovery of market shares after the recession. Traditional

markets, such as the United States and the European Union, experienced slower recoveries, leading to increased imports from faster-recovering emerging markets in Asia and Latin America.

4.1.2 Quarterly macroeconomic data - Federal Reserve Bank of St. Louis

In this section, we analyze the quarter macroeconomic data obtained from the Federal Bank of St. Louis [McCracken and Ng, 2020]. We implement the same of analysis steps as in the previous subsection. The RMSE for one-step ahead prediction in each case is depicted in Table 3, and the top-10 connections in each case are reported in Table 4. spOUTAR performs better than Sparse-VAR in all cases except for the housing group. Furthermore, there was no graphical dependency among the features in the Housing group, and thus we do not report any graphical connectivity for this group.

Table 3: One-step prediction errors of Sparse-VAR and spOUTAR models for different orders of autoregressive processes for FRED-QD data.

Group (USD)	Model	q						
		2	3	4	5	6	7	8
NIPA	Sparse-VAR	0.6177	0.6087	0.7331	0.6496	0.6482	0.6364	0.6829
	spOUTAR	0.6032	0.6162	0.6578	0.9057	0.4048	0.7063	0.4107
Industrial production	Sparse-VAR	24.3526	23.2725	23.7841	23.9199	23.4976	23.1715	22.1972
	spOUTAR	1700.7240	20472.4000	345.1962	5235.3960	1010.423	632.9807	9.4566
Employment and unemployment	Sparse-VAR	1316.0740	1314.5540	1357.4890	1394.3040	1446.8970	1452.6650	1466.6410
	spOUTAR	20.0720	12.8518	9.5959	18.4982	9.4743	11.9983	23641.34
Housing	Sparse-VAR	0.1085	0.0830	0.0775	0.1500	0.0825	0.0920	0.0989
	spOUTAR	0.1176	0.2765	0.1123	0.1703	0.1249	0.1297	0.1201
Prices	Sparse-VAR	41.7861	41.8191	41.8583	41.7098	41.5864	41.5345	41.4844
	spOUTAR	0.3968	0.1667	0.1804	0.1534	2.6356	0.1622	0.7116

We now examine the graphical relationships among factors in two groups: National Income and

Table 4: Edges that exhibit top 10 conditional dependencies in FRED-QD data groups based on the sorted absolute differences in the posterior mean of Ω_{21} .

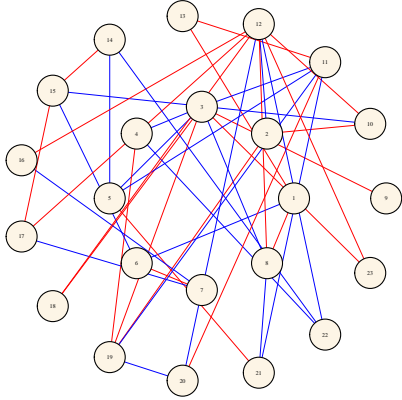
Group	Dependencies (edges)
NIPA	(3, 18), (1, 13), (14, 22), (7, 16), (12, 16), (10, 12), (3, 11), (3, 5), (3, 8), (12, 22)
Industrial production	(14, 16), (14, 15), (11, 14), (4, 14), (1, 14), (10, 14), (5, 14), (2, 14), (6, 14), (7, 14)
Employment and unemployment	(26, 29), (27, 34), (25, 27), (26, 30), (27, 45), (27, 29), (34, 47), (26, 48), (26, 32), (24, 48)
Prices	(21, 46), (24, 38), (7, 46), (24, 41), (11, 19), (10, 20), (7, 34), (3, 23), (12, 38), (37, 42)

Product Accounts (NIPA) and Employment and Unemployment. The graphs for the remaining factors are presented in Appendix A.2. Both groups exhibit a balanced pattern of positive shifts and negative shifts, indicating that the relationships between pairs of factors were reshaped significantly following the 2007–2009 recession. Notably, of the 50 factors analyzed in the third group, the first 23 are related to employment, while the remaining 27 pertain to unemployment. Our analysis reveals that, in general, the relationships among unemployment-related factors were significantly affected by the recession.

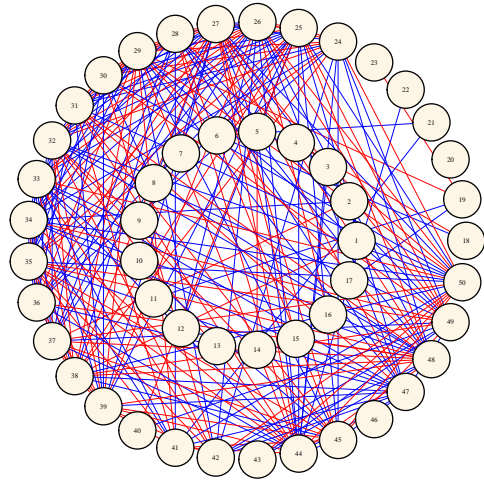
4.2 Simulated data analysis

The focus of this simulation study is to investigate the estimation accuracy of our proposed spOUTAR model and to compare it with a few other potential alternatives. Data is generated under the spOUTAR framework, and we evaluate the model’s performance under both correctly specified and misspecified AR structures in the latent processes. Specifically, we generate the data as follows.

Let n be the number of observations for a p -dimensional time series. The $p \times p$ true precision



(a) Changes in key NIPA indicators, highlighting the largest structural shifts.



(b) Changes in employment and unemployment metrics post recession, showing balanced positive and negative shifts in the labor market.

Figure 5: Impact of the recession on the macroeconomic and labor market indicators in the US economy as revealed by spOUTAR with order 6 in: (a) NIPA attributes and (b) employment/unemployment metrics.

matrix $\mathbf{\Omega}_0$ used to represent the conditional dependence structure of the simulated data is drawn from a graphical Wishart distribution with degrees of freedom 10 and a scale matrix generated from the adjacency matrices of some small-world networks following the Watts-Strogatz model. In this case, we simulate 3 small-world networks, each with 20 nodes are simulated using the `igraph` package in R. Then p time series, each with n observations, are generated using the `arma.sim` function in the `astsa` R package. For the purpose of this study, we consider AR processes with stationarity and causality constraints. Thus, we simulate the partial autocorrelation functions

(PACFs) from $\text{Unif}((-1, -0.9) \cup (0.9, 1))$ distribution and convert them to AR coefficients using the `inla.ar.pacf2phi` function of the INLA package. The autocorrelation functions are generated using `inla.ar.pacf2acf` and the innovation variances of the AR models are specified such that their marginal variances are 1 as mentioned in Section 3. Given the true order q , we construct the $p \times n$ matrix \mathbf{Z} . The same value of q is used to fit the spOUTAR model, thus assuming the order of the AR processes are known. The final data is obtained as $\mathbf{Y} = \mathbf{\Sigma}_0^{1/2} \mathbf{Z}$ where $\mathbf{\Sigma}_0^{1/2}$ is the square root of the inverse of $\mathbf{\Omega}_0$.

4.3 Correctly specified AR orders

In this case, we assume that the true order of the latent AR processes used in the data generation is known, and use the same order to fit a spOUTAR model. We consider three levels of sparsity for $\mathbf{\Omega}_0$, namely, 75%, 90%, and 95%. For each level of sparsity, we choose the dimension of the data, sample size, and the order of the AR processes from the following grid: $p \in \{30, 60, 90\}$, $n \in \{50, 100, 150\}$, and $q \in \{2, 5, 8, 10\}$. We compare the performance of our method with that of GGM and Gaussian copula-based graphical model (GCGM; see Mohammadi et al. [2017]). The average root mean squared error: $\text{RMSE} = \|\bar{\mathbf{\Omega}} - \mathbf{\Omega}_0\|_F/p$ across all experiments for 90% sparsity case is displayed in Table 5, and the results for the other two cases can be found in Appendix A.4.

The GGM yields the poorest performance in all three cases. However, for lower values of q , the GCGM exhibits the best performance in most scenarios. This may be attributed to weaker temporal dependence among observations within individual time series in lower-order AR processes. Furthermore, across different series, copulas are well-known for separating the modeling of marginal distributions from the dependence structure, enabling independent modeling of each variable's distribution while capturing their joint behavior. A less sparse underlying graph further enhances its strong performance. However, as the order of the AR process increases or the underlying

p	n	q	GGM	GCGM	spOUTAR	p	n	q	GGM	GCGM	spOUTAR
30	50	2	6.0377	2.6564	3.4017	30	150	8	26.0452	5.7815	3.7011
30	100	2	10.4520	2.8323	3.7694	30	200	8	33.5753	6.5204	3.7361
30	150	2	14.8057	2.7953	3.7674	30	250	8	41.6565	7.4157	3.8038
60	50	2	5.3626	1.9444	2.2999	60	150	8	19.8279	5.1945	2.7491
60	100	2	8.8180	1.9729	2.6945	60	200	8	25.6120	5.6582	2.6156
60	150	2	12.0416	2.0238	2.6933	60	250	8	31.3362	6.7175	2.6915
90	50	2	5.2464	1.9480	1.8120	90	150	8	17.7364	5.1277	2.2704
90	100	2	7.9137	1.8539	2.2087	90	200	8	21.9630	5.8949	2.2408
90	150	2	9.6735	1.6800	2.3388	90	250	8	26.9005	5.7060	2.3510
30	50	5	8.4568	2.8745	3.5941	30	150	10	27.1173	7.3088	3.7588
30	100	5	15.6330	3.3551	3.5906	30	200	10	35.6630	7.9388	3.8178
30	150	5	22.1923	3.7786	3.6933	30	250	10	43.9372	10.1274	3.7867
60	50	5	7.1477	2.6807	2.5512	60	150	10	20.7453	6.0189	2.6153
60	100	5	12.2996	3.1222	2.7351	60	200	10	26.9059	7.6256	2.7214
60	150	5	20.1701	3.7116	3.2150	60	250	10	32.9758	7.0657	2.5505
90	50	5	6.6208	2.9410	1.9337	90	150	10	18.2535	6.1096	2.1994
90	100	5	10.8862	2.5793	2.2669	90	200	10	23.2690	6.1435	2.2679
90	150	5	15.0431	2.9079	2.3402	90	250	10	28.6306	7.1274	2.1516

Table 5: Correctly-specified AR case: Comparison of average RMSE value in the precision matrix estimation where the true precision is 90% sparse, following a small world networks from the Watts-Strogatz model for different choices of dimension p , sample size n and AR order q .

graphical structure becomes more sparse, our method achieves the best performance.

4.4 Misspecified AR orders

In practice, it is difficult to know the true order of the AR processes. Further, it may happen that all the autoregressions do not exhibit the same degree of dependency on its past observations. Thus,

it is important to assess the credibility of spOUTAR in such situations. We set up a simulation study where the underlying data comes from mixture of ARs of different lag orders. Let m_1, m_2 and m_3 denote the number of simulated AR processes of orders 2, 5, and 8. We vary the numbers m_1, m_2 and m_3 in such a way that every order dominates the other two at some time. The sparsity level of Ω_0 is set at 90%. While training the spOUTAR model, we specify the AR orders for all univariate series to be the same at q and vary it from 2 through 8.

Table 6 illustrates the results obtained from the simulation. It is clear that the proposed method delivers the best performance across all the cases. As the temporal dependencies among observations in each time series get more complex, the GCGM fails to perform well, likely because it cannot capture higher-order temporal dependencies.

q	m	GGM	GCGM	spOUTAR	m	GGM	GCGM	spOUTAR	m	GGM	GCGM	spOUTAR
2	(30, 15, 15)	11.3004	2.9574	2.6534	(15, 30, 15)	11.9860	3.4435	2.6379	(15, 15, 30)	12.2606	3.8291	2.6708
3	(30, 15, 15)	11.1240	3.3355	2.7101	(15, 30, 15)	12.1674	3.5209	2.7009	(15, 15, 30)	12.2681	3.9956	2.6240
4	(30, 15, 15)	11.2707	3.4013	2.6024	(15, 30, 15)	12.0825	3.3375	2.7458	(15, 15, 30)	12.3202	3.6375	2.6937
5	(30, 15, 15)	11.1912	3.5026	2.9191	(15, 30, 15)	11.8330	3.2521	2.7774	(15, 15, 30)	12.2782	3.8517	2.6693
6	(30, 15, 15)	11.3114	3.2632	2.6638	(15, 30, 15)	11.8977	3.3793	2.8290	(15, 15, 30)	12.4350	3.6204	2.6603
7	(30, 15, 15)	11.3305	3.1309	2.7027	(15, 30, 15)	12.1298	3.5228	3.2474	(15, 15, 30)	12.2040	3.6489	2.6879
8	(30, 15, 15)	11.2302	3.1590	2.6862	(15, 30, 15)	11.9044	3.2057	2.7256	(15, 15, 30)	12.3466	3.7656	2.7221

Table 6: Misspecified AR case: Comparing average RMSE of the precision matrix estimates, where the latent AR processes are generated by combining m_1 time series of order 2, m_2 time series of order 5, and m_3 time series of order 8; denoted by the tuple $m := (m_1, m_2, m_3)$. The sparsity level of the true precision is set at 90%. spOUTAR is fitted setting q as the order for all the univariate series.

5 Discussion

This article presents a novel model to estimate the underlying conditional dependency structure in multivariate time series data, and good predictive performance. Based on the simulation studies, spOUTAR outperforms its competitors particularly when the data has high temporal correlation among its observations, or the underlying graphical structure is very sparse. Furthermore, the proposed model demonstrates superior predictive performance in all real data analyses, effectively estimating significant changes in relationships among macroeconomic factors in the US and among GDP and related components in OECD countries following the Great Recession (2007–2009). As an extension to this work, it would be interesting to see how the spOUTAR model performs with univariate latent nonlinear autoregressive processes.

Funding

The authors would like to thank the National Science Foundation collaborative research grants DMS-2210280 (Shuvrarghya Ghosh, Subhashis Ghosal) / 2210281 (Anindya Roy) / 2210282 (Arkaprava Roy).

References

- L. Ball. Long-term damage from the great recession in oecd countries. *European Journal of Economics and Economic Policies*, 11(2):149–160, 2014.
- S. Basu and G. Michailidis. Regularized estimation in sparse high-dimensional time series models. *The Annals of Statistics*, pages 1535–1567, 2015.

- Q. Cai, J. Kang, and T. Yu. Bayesian network marker selection via the thresholded graph laplacian gaussian prior. *Bayesian analysis*, 15(1):79, 2020.
- F. Cordoni and A. Sancetta. Consistent causal inference for high-dimensional time series. *Journal of Econometrics*, 246(1-2):105902, 2024.
- V. Gómez-Rubio. *Bayesian inference with INLA*. Chapman and Hall/CRC, 2020.
- H. Haario, E. Saksman, and J. Tamminen. An adaptive metropolis algorithm. *Bernoulli*, 7(2): 223–242, 2001.
- L. A Jacobsen and M. Mather. Us economic and social trends since 2000. *Population Bulletin*, 65 (1), 2010.
- A. L. Kalleberg and T. M. Von Wachter. The us labor market during and after the great recession: Continuities and transformations. *RSF: The Russell Sage Foundation Journal of the Social Sciences*, 3(3):1–19, 2017.
- Helmut Lütkepohl. *Introduction to multiple time series analysis*. Springer Science & Business Media, 2013.
- M. McCracken and S. Ng. Fred-qd: A quarterly database for macroeconomic research. Technical report, National Bureau of Economic Research, 2020.
- A. Mohammadi, F. Abegaz, E. Heuvel, and E. C. Wit. Bayesian modelling of dupuytren disease by using gaussian copula graphical models. *Journal of the Royal Statistical Society Series C: Applied Statistics*, 66(3):629–645, 2017.
- R. Mohammadi and E. C Wit. Bdgraph: An r package for bayesian structure learning in graphical models. *arXiv preprint arXiv:1501.05108*, 2015.

- R. Mohammadi and E. C Wit. Bdgraph: An r package for bayesian structure learning in graphical models. *Journal of Statistical Software*, 89:1–30, 2019.
- G. O. Roberts and O. Stramer. Langevin diffusions and metropolis-hastings algorithms. *Methodology and computing in applied probability*, 4:337–357, 2002.
- A. Roy, A. Roy, and S. Ghosal. Bayesian inference for high-dimensional time series by latent process modeling. *arXiv preprint arXiv:2403.04915*, 2024.
- J. Song and T. M. Von Wachter. Long-term nonemployment and job displacement. In *Jackson Hole Economic Symposium Conference Proceedings Kansas City Federal Reserve Board*, 2014.
- J. H. Stock and M. W. Watson. Forecasting with many predictors. *Handbook of economic forecasting*, 1:515–554, 2006.
- J. H. Stock and M. W. Watson. Disentangling the channels of the 2007-2009 recession. Technical report, National Bureau of Economic Research, 2012.

A Appendix

A.1 Computation of the gradients

In this section, we derive the gradients of the joint log-likelihood function of p $\text{AR}(q)$ processes, each having n observations, with respect to \mathbf{L} and \mathbf{D} . Without loss of generality, we set $\mathbf{\Omega}_1 = \mathbf{\Omega}_2 = \mathbf{\Omega}$ for simpler computations. In case of two precision matrices, we set $\mathbf{Z} = \mathbf{Z}_1$ in the computations detailed in Section [A.1.1](#). Subsequently, utilize the result in Section [A.1.2](#) to obtain the gradient with respect to \mathbf{L}_1 . Likewise, the gradient of \mathbf{L}_2 can be computed taking $\mathbf{Z} = \mathbf{Z}_2$. The notation

$\nabla_{\mathbf{X}}f$ denotes the vector differential operator that computes the gradient of a function $f : \mathbb{R}^d \rightarrow \mathbb{R}$ with respect to $\text{vec}(\mathbf{X})$. Lastly, we define $\text{vec}^{-1} : \mathbb{R}^{mn} \rightarrow \mathbb{R}^{m \times n}$ as an inverse vectorization map.

A.1.1 Gradient with respect to \mathbf{Z}

The joint log-likelihood function of all latent AR processes of order K is expressed as

$$\log \pi(\Psi, \boldsymbol{\sigma} | \mathbf{Z}) = - \sum_{i=1}^p \frac{1}{2\sigma_i^2} \sum_{t=q+1}^n (Z_{i,t} - \sum_{k=1}^q \varphi_{i,k} Z_{i,t-k})^2.$$

The derivative of this function with respect to \mathbf{Z} is a matrix of dimensions $p \times n$ whose (i, t) th entry is computed as follows.

$$(\nabla_{\mathbf{Z}} \log \pi(\Psi, \boldsymbol{\sigma} | \mathbf{Z}))_{i,t} = \begin{cases} -\frac{1}{\sigma_i^2} (Z_{i,t} - \sum_{k=1}^q \varphi_{i,k} Z_{i,t-k}) \\ + \sum_{j=1}^{\min(N-t, q)} \frac{1}{\sigma_i^2} (Z_{i,t+j} - \sum_{k=1}^q \varphi_{i,k} Z_{i,t+j-k}) \varphi_{i,k}, & t > q, \\ \frac{1}{\sigma_i^2} (Z_{i,q+1} - \sum_{k=1}^q \varphi_{i,k} Z_{i,q+1-k}) \varphi_{i,k}, & t \in [q]. \end{cases}$$

A.1.2 Gradient with respect to \mathbf{L}

We know $\boldsymbol{\Omega}^{1/2} = \mathbf{D}(\mathbf{I} - \mathbf{L})$ such that $\mathbf{Z} = \mathbf{U}^T \mathbf{D}(\mathbf{I} - \mathbf{L}) \mathbf{Y}$. Vectorizing both sides of the latter equation, we have $\text{vec}(\mathbf{Z}) = \text{vec}(\mathbf{U}^T \mathbf{D} \mathbf{Y}) - \text{vec}(\mathbf{U}^T \mathbf{D} \mathbf{L} \mathbf{Y})$ and $\text{vec}(\mathbf{U}^T \mathbf{D} \mathbf{L} \mathbf{Y}) = [\mathbf{Y}^T \otimes \mathbf{U}^T \mathbf{D}] \text{vec}(\mathbf{L})$.

Since $\nabla_{\mathbf{L}} \text{vec}(\mathbf{Z}) = -(\mathbf{Y}^T \otimes \mathbf{U}^T \mathbf{D})$, by the chain rule of differentiation, we obtain

$$\nabla_{\mathbf{L}} \log \pi(\Psi, \boldsymbol{\sigma} | \mathbf{Z}) = -\text{vec}^{-1} \left[[\mathbf{Y} \otimes \mathbf{D} \mathbf{U}] \times \text{vec}(\nabla_{\mathbf{Z}} \log \pi(\Psi, \boldsymbol{\sigma} | \mathbf{Z})) \right].$$

A.1.3 Gradient with respect to $\log(\mathbf{D})$

We can write $\text{vec}(\mathbf{Z}) = [\mathbf{Y}^T (\mathbf{I} - \mathbf{L})^T \otimes \mathbf{U}^T] \text{vec}(\mathbf{D})$. Differentiating both sides with respect to \mathbf{D} , we have $\nabla_{\mathbf{D}} \text{vec}(\mathbf{Z}) = \mathbf{Y}^T (\mathbf{I} - \mathbf{L})^T \otimes \mathbf{U}^T$, where \otimes denotes the Kronecker product, and $\nabla_{\log \mathbf{D}} \text{vec}(\mathbf{D}) =$

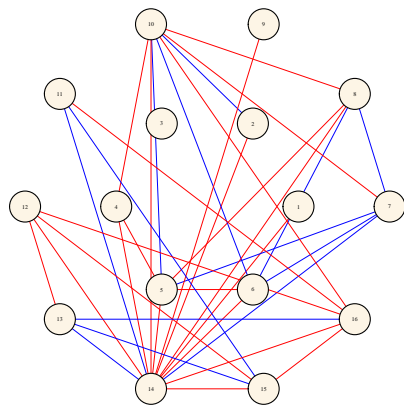
$\text{vec}(\mathbf{D})$. By the chain-rule, we obtain

$$\nabla_{\log \mathbf{D}} \log \pi(\Psi, \sigma | \mathbf{Z}) = \text{vec}^{-1} \left[((\mathbf{I} - \mathbf{L})\mathbf{Y} \otimes \mathbf{U}) \text{vec}(\nabla_{\mathbf{Z}} \log \pi(\Psi, \sigma | \mathbf{Z})) \right] \odot \mathbf{D},$$

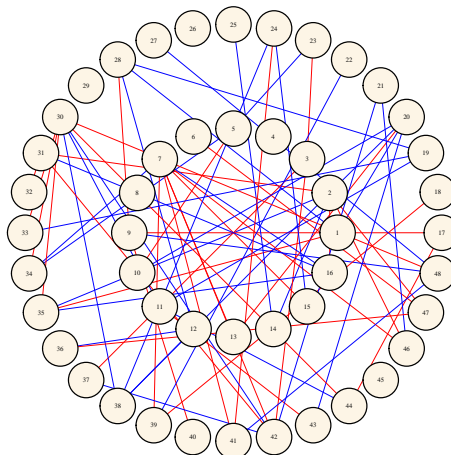
where \odot represents the Hadamard product of two matrices. Note that in the Langevin Monte Carlo steps, we evaluate the negative of the log likelihood function and its gradient.

A.2 Supplementary results: FRED-QD data analysis

The graphs for Industry attributes and Prices attributes are presented in Figure 6a and Figure 6b respectively.



(a) Shifts in industrial production indicators, showing sector-specific output changes, as revealed by spOUTAR with order 8.



(b) Shifts in price-related attributes (inflation, CPI components), as revealed by spOUTAR with order 7.

Figure 6: Economic impact of the 2009 recession on: (a) industrial output, (b) price changes across sectors.

A.3 Supplementary results: OECD data analysis

ID	Country	ID	Country	ID	Country	ID	Country	ID	Country
ISL	Iceland	NOR	Norway	CHE	Switzerland	GBR	United Kingdom	NLD	Netherlands
MEX	Mexico	LVA	Latvia	CHL	Chile	SWE	Sweden	ZAF	South Africa
ITA	Italy	FRA	France	DNK	Denmark	SVN	Slovenia	CAN	Canada
CRI	Costa Rica	BGR	Bulgaria	IRL	Ireland	LUX	Luxembourg	ROU	Romania
USA	United States	NZL	New Zealand	SVK	Slovakia	EST	Estonia	IND	India
GRC	Greece	CZE	Czech Republic	AUT	Austria	DEU	Germany	POL	Poland
TUR	Turkey	HUN	Hungary	ESP	Spain	ISR	Israel	HRV	Croatia
BEL	Belgium	AUS	Australia	PRT	Portugal	IDN	Indonesia	COL	Colombia
BRA	Brazil	KOR	South Korea	FIN	Finland	JPN	Japan	LTU	Lithuania

Table 7: List of countries analyzed in OECD data with their ISO 3166 country codes.

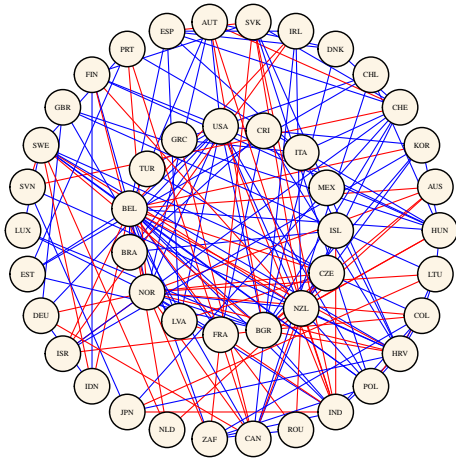
We report some additional results related to Section 4.1 in this section. The general government expenditure of a country primarily comprises individual expenditures: spending on services provided to specific individuals, such as healthcare or education, and; collective expenditures: spending on services benefiting the community as a whole, like defense, justice, or public administration. In Figure 7a, we can observe a rich dependency structure in the government expenditure of OECD countries, consisting of many positive and negative shifts. Such changes in relationships indicate the formation of new trade agreements, changes to existing trade policies, and similar welfare systems — giving rise to new trade partnerships and decreasing the reliance on the traditional markets.

A.4 Supplementary results: simulated data analysis

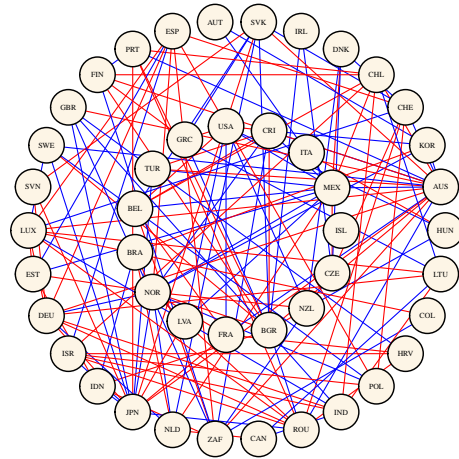
The comparison of performance of GGM, GCGM, and spOUTAR, for the 75% sparsity level of Ω_0 is displayed in Table 8 whereas that for sparsity level 95% is shown in Table 9.

p	n	q	GGM	GCGM	spOUTAR	p	n	q	GGM	GCGM	spOUTAR
30	50	2	5.7663	2.7016	3.5120	30	150	8	26.1881	5.5204	3.9208
30	100	2	9.8990	2.8385	3.9385	30	200	8	33.7859	7.3007	3.8094
30	150	2	13.0946	3.0159	3.9237	30	250	8	41.0031	7.2416	3.9751
60	50	2	4.8553	3.0263	4.0939	60	150	8	18.7041	4.9537	4.5559
60	100	2	7.8095	3.0808	4.3947	60	200	8	24.6697	6.2315	4.4261
60	150	2	10.5585	3.2697	4.4669	60	250	8	29.9310	6.0104	4.4599
90	50	2	4.9125	2.7682	3.4992	90	150	8	16.8037	4.7577	3.6718
90	100	2	7.5720	2.7268	3.6915	90	200	8	22.1458	5.8282	3.5927
90	150	2	9.7087	2.5876	3.6159	90	250	8	25.8131	6.2915	3.9384
30	50	5	8.3758	2.9174	3.7243	30	150	10	27.1034	6.7129	3.8547
30	100	5	15.5352	3.4515	3.8630	30	200	10	35.3740	8.7824	3.8439
30	150	5	22.0368	4.0451	3.9490	30	250	10	44.1561	9.4918	3.8736
60	50	5	6.4550	3.2296	4.2286	60	150	10	19.8073	5.6529	4.4585
60	100	5	11.4006	3.5430	4.4444	60	200	10	25.9693	7.2165	4.3956
60	150	5	16.1652	3.7312	4.4626	60	250	10	31.8303	7.4142	4.4025
90	50	5	6.3952	3.1627	3.5848	90	150	10	8.9084	3.5498	1.8847
90	100	5	10.5872	3.4964	3.7118	90	200	10	22.7985	6.5974	3.7353
90	150	5	14.7463	3.7244	3.5480	90	250	10	27.7146	8.1353	3.7046

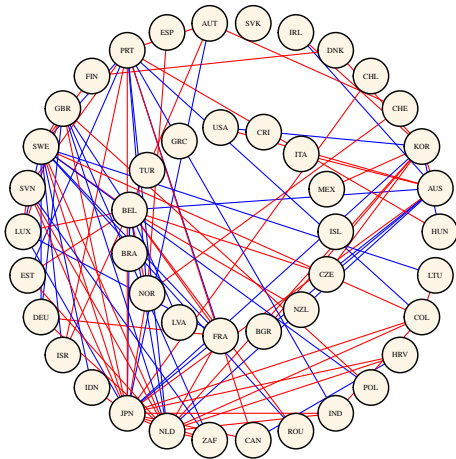
Table 8: Correctly-specified AR case: Comparison of average RMSE value in the precision matrix estimation where the true precision is 75% sparse, following a small world networks from the Watts-Strogatz model for different choices of dimension p , sample size n , and AR order q .



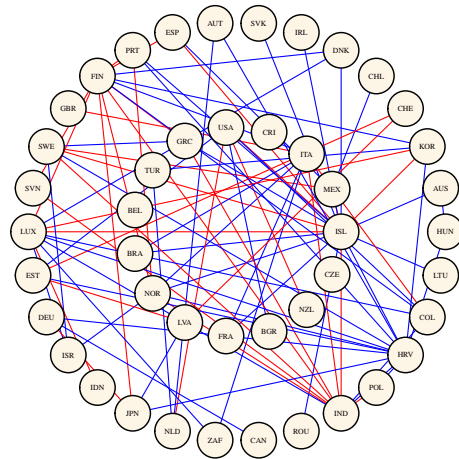
(a) Changes in government expenditure indicators, highlighting fiscal shifts; using spOUTAR with order 4.



(b) Shifts in total GDP, highlighting overall economic impact; using spOUTAR with order 2.



(c) Changes in household and non-profit organization expenditures, showing consumption adjustments; using spOUTAR with order 3.



(d) Changes in capital investment and fixed asset indicators, illustrating investment trends; using spOUTAR with order 3.

Figure 7: Post-2009 recession structural shifts in: (a) government expenditure, (b) household/non-profit expenditure, (c) total GDP, and (d) capital investments.

p	n	q	GGM	GCGM	spOUTAR	p	n	q	GGM	GCGM	spOUTAR
30	50	2	6.1040	2.1191	2.5444	30	150	8	26.7892	5.7238	2.8982
30	100	2	10.3034	2.2287	2.8205	30	200	8	34.4414	6.6932	2.9884
30	150	2	13.2441	2.3665	2.7987	30	250	8	41.9731	6.8604	2.8952
60	50	2	5.8100	1.7967	1.7293	60	150	8	20.4444	5.1302	2.1133
60	100	2	8.7152	1.7201	2.1147	60	200	8	25.9356	5.4493	2.1940
60	150	2	11.3598	1.7186	2.1767	60	250	8	31.4138	6.1560	2.0539
90	50	2	5.2888	1.8296	1.6129	90	150	8	17.5272	4.8658	1.5902
90	100	2	7.9315	1.5605	1.5725	90	200	8	22.6506	5.4356	1.7678
90	150	2	10.4298	1.4095	1.9111	90	250	8	26.7136	6.6242	1.8346
30	50	5	9.0106	2.5357	2.6028	30	150	10	27.7238	7.7051	2.7569
30	100	5	16.1381	3.0613	2.8607	30	200	10	36.3130	7.4012	2.8068
30	150	5	22.8368	3.7322	2.8863	30	250	10	44.3195	8.9971	2.8235
60	50	5	7.6580	2.7688	1.9800	60	150	10	21.1959	6.2402	2.1510
60	100	5	12.8130	2.9516	2.1114	60	200	10	27.0981	7.9321	2.3463
60	150	5	17.5129	3.1878	2.0956	60	250	10	33.1425	9.0242	2.1189
90	50	5	6.9174	3.0060	1.4958	90	150	10	32.1654	7.0407	1.4259
90	100	5	11.3200	2.6949	1.8013	90	200	10	30.9774	8.1224	1.3153
90	150	5	14.9809	2.4116	1.7804	90	250	10	28.2674	6.7610	1.9941

Table 9: Correctly-specified AR case: Comparison of average RMSE value in the precision matrix estimation where the true precision is 95% sparse, following a small world networks from the Watts-Strogatz model for different choices of dimension p , sample size n and AR order q .